Earth and Planetary Science Letters 271 (2008) 254–266

Contents lists available at ScienceDirect

Earth and Planetary Science Letters

journal homepage: www.elsevier.com/locate/epsl

Seawater pH, pCO_2 and $[CO_3^{2-}]$ variations in the Caribbean Sea over the last 130 kyr: A boron isotope and B/Ca study of planktic foraminifera

G.L. Foster *

Bristol Isotope Group, Department of Earth Sciences, Bristol University, Wills Memorial Building, Queens Rd, Bristol BS8 1RJ, United Kingdom

ARTICLE INFO

Article history:
Received 14 December 2007
Received in revised form 7 April 2008
Accepted 10 April 2008
Available online 24 April 2008

Editor: H. Elderfield

Keywords:
Boron isotopes
pH
proxy
pCO_2
carbonate ion concentration
Caribbean Sea
calibration

ABSTRACT

Here a new analytical methodology is described for measuring the isotopic composition of boron in foraminifera using multicollector inductively coupled plasma mass spectrometry (MC-ICPMS). This new approach is fast (~10 samples analysed in duplicate per analytical session) and accurate (to better than 0.25‰ at 95% confidence) with acceptable sample size requirements (1–3 mg of carbonate). A core top calibration of several common planktic and two benthic species from geographically widespread localities shows a very close agreement between the isotopic composition measured by MC-ICPMS and the isotopic composition of $B(OH)_4^-$ in seawater (as predicted using the recently measured isotopic equilibrium factor of 1.0272) at the depth of habitat. A down core and core top investigation of boron concentration (B/Ca ratio) shows that the partition coefficient is influenced by $[CO_3^{2-}]$ complicating the application of this proxy. Nevertheless, it is demonstrated that these two proxies can be used to fully constrain the carbonate system of surface water in the Caribbean Sea (ODP Site 999A) over the last 130 kyr. This reconstruction shows that during much of the Holocene and the last interglacial period surface water at Site 999A was in equilibrium with the atmosphere with respect to CO_2. During the intervening colder periods although the surface water pCO_2 was lower than the Holocene, it was a minor to significant source of CO_2 to the atmosphere possibly due to either an expansion of the eastern equatorial Atlantic upwelling zone, or a more local expansion of coastal upwelling in the southern Caribbean. Such reorganisation of the oceanic carbonate system in favour of a larger source of CO_2 to the atmosphere from the equatorial ocean may require mechanisms responsible for lowering atmospheric CO_2 during glacial periods to be more efficient than previously supposed.

1. Introduction

The exact cause(s) of the well documented variations in atmospheric CO_2 that have accompanied the growth and decay of ice sheets throughout the Quaternary (Petit et al., 1999; Siegenthaler et al., 2005) remains elusive. Of all the carbon reservoirs on Earth, only the oceans have a large enough store of carbon and a fast enough exchange rate with the atmosphere to explain these glacial–interglacial variations in CO_2 (e.g. Sigman and Boyle, 2000). The concentration of CO_2 in the atmosphere is determined by a balance between regions of the surface ocean that act as sinks (mainly cold, high latitude regions where water itself sinks) and areas that act as sources (mainly warm low latitude regions where relatively old water, rich in respired nutrients, is upwelled back to the surface). The mechanism that results in the ocean taking up more CO_2 during glacial periods is unknown (e.g. Archer et al., 2000; Sigman and Boyle, 2000) but most likely involves a complex interplay of a number of processes (e.g. see Brovkin et al., 2007) which serve to alter the magnitude of the various oceanic sinks and sources of CO_2 to the atmosphere (e.g. Sigman and Boyle, 2000; Toggweiler et al., 2006; Brovkin et al., 2007).

The ocean carbonate system consists of a number of co-varying parameters, two of its six independent parameters (pH, $[CO_2]$, $[HCO_3^-]$, $[CO_3^{2-}]$, total alkalinity – TA and total dissolved carbon – DIC) must to be known to fully describe changes in the system. Ideally then, proxies for two or more of these variables in the past are required. A number of studies have shown that the isotopic composition of boron (Hemming and Hanson, 1992; Sanyal et al., 1995; Pearson and Palmer, 2000; Hönisch and Hemming, 2005) and its concentration in foraminifera (Yu et al., 2007a; Ni et al., 2007) can fulfil this role. The combined use of these proxies offers the opportunity to completely reconstruct the state of the paleo-carbonate system and hence establish how the saturation state of the oceans with respect to CO_2 changed in the past. In this contribution the fidelity of the coupled boron based proxies is examined and their utility is demonstrated by a down core study of the Caribbean over the last 130 kyrs.

* Tel.: +44 117 9545377; fax: +44 117 9253385.
E-mail address: g.l.foster@bristol.ac.uk.

0012-821X/$ – see front matter © 2008 Elsevier B.V. All rights reserved.
doi:10.1016/j.epsl.2008.04.015

2. Methods

2.1. Boron geochemical proxies for the ocean carbonate system

2.1.1. Boron concentration

In aqueous solutions boron exists as two species, boric acid [$B(OH)_3$] and borate ion [$B(OH)_4^-$] the proportions of which are pH dependant as defined by the following equilibrium:

$$B(OH)_3 + H_2O \leftrightarrow B(OH)_4^- + H+ \quad (1)$$

The equilibrium constant is defined as:

$$K_B^* = \frac{[H^+][B(OH)_4^-]}{[B(OH_3)]} \quad (2)$$

The K_B^* of seawater has been determined experimentally and pK_B^* is 8.5975 at 25 °C and a salinity of 35 psu (DOE, 1994).

The abundance of boron in biologically precipitated and inorganic carbonates has been observed to increase with increasing pH (Hemming and Hanson, 1992; Sanyal et al., 2000), which is consistent with a model in which only the charged species, $B(OH)_4^-$, is incorporated into calcium carbonate. Hemming and Hanson (1992) proposed the following mechanism for the substitution of boron into carbonate:

$$CaCO_3 + B(OH)_4^- \leftrightarrow Ca(HBO_3) + HCO_3^- + H_2O \quad (3)$$

The exchange distribution coefficient, K_D, for B substitution into calcium carbonate can be expressed as:

$$K_D = \frac{[B/Ca]_{solid}}{[B(OH)_4^-/HCO_3^-]_{seawater}} \quad (4)$$

This model thus predicts that the concentration of boron in marine carbonates (or more strictly, the B/Ca ratio) will be a function of the ratio of $[B(OH)_4^-]/[HCO_3^-]$ in seawater, which is pH dependant (see Yu and Elderfield, 2007a). Given a good calibration of K_D it is therefore possible to use measured foraminiferal B/Ca to reconstruct seawater $[B(OH)_4^-/HCO_3^-]$. Importantly, if the $[B(OH)_4^-]$ is known through an independent reconstruction of pH, as is possible using boron isotopes (see below), an estimate of $[HCO_3^-]$ can be made, allowing the carbonate system to be fully constrained.

Although studies of B/Ca in foraminifera are in their infancy, two recent studies have investigated the controls of boron incorporation into planktic species (e.g. Yu et al., 2007a; Ni et al., 2007). These contributions both suggest that the substitution mechanism outlined above (Eq. (3)) appears reasonable but the K_D is not constant between foraminifera species. The K_D was also found to vary within an individual species in response to changes in foraminiferal growth rate (Ni et al., 2007), temperature and/or carbonate ion concentration (Yu et al., 2007a) over and above the effects of these latter two parameters on speciation within the carbonate system. The mechanism(s) responsible for this behaviour has yet to be identified.

2.1.2. Boron isotopes

Boron has two isotopes, ^{10}B and ^{11}B, and in common with most stable isotope systems variations in boron isotopes are expressed in a delta notation relative to a standard, in this case NIST SRM 951 boric acid ($^{11}B/^{10}B = 4.04367$; Catanzaro et al., 1970) as follows:

$$\delta^{11}B = \left[\left(\frac{^{11}B/^{10}B_{sample}}{^{11}B/^{10}B_{NIST951}}\right) - 1\right] \times 1000 \quad (5)$$

Due to differences in coordination and consequent B–O vibrational frequencies there is a pronounced isotopic fractionation ($\alpha_{4-3} = 1/^{11-10}K_B$) between the two aqueous species of boron (Kakihana et al., 1977). If only the charged species is incorporated into carbonate (Eq. (3)), and given that the proportions of the species changes according to pH, the isotopic composition of boron in marine carbonate should also be pH dependent. The magnitude of this isotopic fractionation has been a subject of much debate (e.g. Pagani et al., 2005; Zeebe, 2005) with empirical and theoretical estimates of $^{11-10}K_B$ ranging from 1.0176 (Sanchez-Valle et al., 2005) to ≥1.030 (Zeebe, 2005). The consequent uncertainty in the exact value of $^{11-10}K_B$ has been cited as a limiting factor in the applicability of this proxy (Pagani et al., 2005). However, the $^{11-10}K_B$ in seawater has recently been determined experimentally for the first time (Klochko et al., 2006). Using a spectrophotometric approach, Klochko et al. (2006) determined that the $^{11-10}K_B$ in seawater is largely independent of temperature and has a value of 1.0272 ± 0.0006 ($S = 35$, $B_T = 0.01$ mol kg^{-1}). This value is significantly different from the theoretically estimated value commonly used (i.e. 1.0194, Kakihana et al., 1977) for paleoceanographic applications (e.g. Hönisch et al., 2007) but this now allows an accurate prediction of the isotopic composition of $B(OH)_4^-$ in seawater and hence an examination of whether pH dependant inorganic isotopic fractionation is the dominant control on the boron isotopic composition of boron in marine carbonates.

Although the theory behind the boron isotope pH proxy is relatively well established and is now well placed in an experimental framework, accurate pH reconstructions are still dependant on accurate measurements of $\delta^{11}B$. The accurate measurement of isotope ratios in systems with only two stable nuclides is a difficult task due to the lack of a ready means of correction for mass spectrometer induced mass fractionation. This, coupled with the low concentration of boron in foraminifera (~10 ppm), has led inter-laboratory biases well beyond the required precision (better than 0.5‰). For instance, Foster et al. (2006) reviewed the $\delta^{11}B$ reported by different laboratories for the same species of Holocene foraminifera from similar locations, and noted that values ranged from 22 to 26‰ (8 times the required precision). This level of disagreement is most likely due to analytical difficulties and in particular the influence of sample matrix on NTIMS (negative ion thermal ionisation mass spectrometry) measurements. With rigorous measurement protocols it is possible to generate good quality, self-consistent data for samples with the same matrix by NTIMS (e.g. Hönisch and Hemming, 2005), but in this contribution I describe a new analytical methodology that removes the matrix before analysis and so overcomes such problems.

2.2. Sample preparation, sampling locations, and trace element analysis

The new technique was calibrated using a number of Holocene core top samples predominantly from mid- and low-latitudes as listed in Table 1 and shown in Fig. 1. The Holocene age of these core tops was verified using oxygen isotope stratigraphy and published age models (see Table 1). Additional support for the Holocene age of the sediments sampled comes from $\delta^{18}O$ measurements of the analysed foraminifera which exhibit values that are typical of Holocene aged samples (Table 2). From a selection of these samples, depending on abundance, three species of planktic foraminifera were hand separated from three size fractions: *Neogloboquadrina dutertrei* (425–500 μm), *Globigerinoides sacculifer* (with final sac-like chamber; 500–600 μm), *Globigerinoides ruber* (white; 300–355 μm). From two further sites (BOFS11K and BOFS17K) picked benthic epifaunal foraminiferal species *Cibicidoides mundulus* (250–500 μm; BOFS17K) and *Cibicidoides wuellerstorfi* (250–500 μm; BOFS11K) were provided by Jimin Yu (Cambridge University). The new methodology was also used in a 'down core' study of *G. ruber* (white; 300–355 μm) at ODP Site 999A (Leg 165) in which thirty samples from the last 130 kyr were selected according to the age

Table 1
Sample site locations for core top calibration

Site	ODP leg	Depth (cm bs)	Long (E)	Lat (N)	Core WD (m)	Ω $CaCO_3$	Ω $CaCO_3$ WD [a] (m)	Sed. rate [b] (cm/kyr)	Age [c] (kyr)	Age model
847B	138	6–9	−95.32	0.20	3334	0.88	3454	4.6	1.3–2.0	Shackleton et al. (1995)
851B	138	2–4	−110.57	2.77	3760	0.88	3454	2.1	1.0–1.9	Shackleton et al. (1995)
925B	154	6–8	−43.48	4.20	3040	1.47	2964	4.7	1.3–1.7	Bickert et al. (1997)
664C	108	8–10	−23.23	0.10	3806	0.98	4136	3.6	2.9–3.6	Raymo et al. (1997)
668B	108	0–2	−20.93	4.77	2693	1.44	2651	1.6	0–1.1	Bird and Cali (2002)
999A	165	4–5	−78.73	12.75	2828	1.51	2718	3.7	3.9–4.0	Schmidt et al. (2004)
806B	130	12–17	159.37	0.32	2520	1.03	2564	2.9	7.3–8.6	Lea et al. (2000)
GeoB4216-1		3	−12.40	30.63	2324	1.56	2418	5.0	2.0	Freudenthal et al. (2002)
GeoB1208-1		5	7.11	−24.49	2971	1.33	2955	3.2	1.6	Thiessen and Bleil (2002)
BOFS-11K		0–1	−20.35	55.19	2004	2.06	1624	1.92	0.0–0.5	Manighetti and McCave (1995)
BOFS-17K		2	−16.50	58.00	1150	2.39	1186	3.9	1.5	Barker et al. (2004)

[a] Water depth of nearest deepwater GLODAP station used to calculate omega—the CaCO saturation state.
[b] Sedimentation rate over the last ~20 kyr.
[c] Age in kyr according to cited age model.

model of Schmidt et al. (2004). The highest sampling density was over the last 26 kyr.

Samples of 1–3 mg of foraminiferal carbonate (e.g. 170 tests of *G. ruber* of 300–355 μm) were cleaned following standard cleaning techniques used for boron isotope analysis (see Ni et al., 2007). Briefly, after crushing the foraminifers between pre-cleaned glass plates, clay was removed following the approach outlined by Barker et al. (2003). Since boron is not present in high concentrations in Fe–Mn oxides, a reductive cleaning step (e.g. Boyle and Keigwin, 1985/86) was not carried out (see Yu et al., 2007b). Following other boron isotope studies (e.g. Hönisch and Hemming, 2005) organic material was oxidised by bleaching the samples overnight in sodium hypochlorite (NaClO; 5% Cl). Once cleaned the foraminifers were transferred to acid-cleaned screw-top 5 ml Teflon beakers and dissolved in 100–300 μl (depending on sample size) of Teflon-distilled 0.5 M HNO_3. A small aliquot of this dissolved sample (~5% by volume) was taken and analysed for trace elements (Ca, Mg, Sr, Na, Mn, Li, B, Ba, Cd, U, Al, Cu, Fe, Nd and Zn) on a Thermo Finnigan Element 2 ICP-MS following the approach detailed in Ni et al. (2007), with the exception that the Ca concentration of samples and standards were matched, negating the need for a matrix correction. The B/Ca ratio determined using this approach is precise and accurate to 5% (at 95% confidence), as determined by isotope dilution analyses and as evidenced by the reproducibility of >30 measurements of an in-house coral standard (B/Ca = 192.7 ± 5.6 μmol/mol; 2 s.d.). This ICP-MS determination of trace elements was also used to examine the efficiency of the clay removal step during cleaning. In all cases the data presented here have Al/Ca ratios of <120 μmol/mol and typically <50 μmol/mol.

2.3. Boron isotopic analysis by MC-ICPMS

The isotopic composition of the foraminifers was determined with a new methodology developed at the University of Bristol using a Thermo Finnigan Neptune MC-ICPMS. A full description of this methodology can be found in the Online supplementary material accompanying this contribution. The MC-ICPMS approach has a number of advantages over the standard NTIMS approaches more commonly used for measuring foraminifera. Of principal importance is the relative stability of machine induced mass fractionation that is easily corrected for by a sample-standard bracketing approach. For the best quality data, in common with other isotopic systems measured by MC-ICPMS, it is necessary to first remove the samples $CaCO_3$ matrix and concentrate the boron using anionic exchange resin. MC-ICPMS is less sensitive than NTIMS which, along with the blank associated with boron separation, means sample sizes are slightly larger (i.e. 1–3 mg of foraminiferal calcite). This sample requirement is by no means limiting and the benefits of controlling mass fractionation by using MC-ICPMS and removing sample matrix are clear—complete procedural replicates of seawater and an in-house coral standard demonstrate that the reproducibility of this approach is ±0.25‰ at a 95% confidence level (see the Online supplementary material). It should be noted that in contrast to TIMS measurements, this estimate of uncertainty also incorporates any uncertainty relating to standardisation of each analysis to NIST SRM 951.

2.4. Input parameters for calibration

For the core top calibration it is necessary to compare the $\delta^{11}B$ and the B/Ca ratio of the measured foraminifera to pre-industrial ocean carbonate

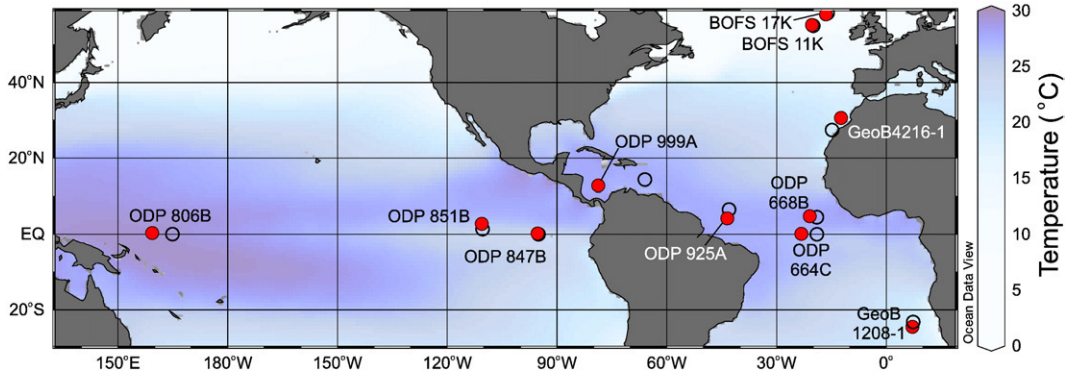

Fig. 1. Map showing the locations of cores used in this study (filled red circles). Open circles show the locations of the GLODAP sites used for temperature, salinity, and pre-industrial carbonate system parameters. Note that in some cases the GLODAP site location overlaps with that of the core location and may not be visible. Site locations are overlain on a map of mean annual SST from the WOA05 database. (For interpretation of the references to colour in this figure legend, the reader is referred to the web version of this article.)

Table 2
B/Ca and d11B data for three species of planktic foraminifera from a variety of core top locations

Site[a]	Temp	S	pH	$[CO_3^{2-}]$	$\Delta^{11}B$ $B(OH)_4^-$	$[B(OH)_4^-/HCO_3^-]$	$\delta^{18}O$[c]	$\delta^{11}B$								B/Ca[b]	Kd*1000
	(°C)	(psu)		(μmol/kg)				1	2 s.e.	2	2 s.e.	3	2 s.e.	Av.	95%[d]	(μmol/mol)	
G. rubber (white, 300–355 μm)																	
847B[e]	20.71	34.68	8.119	214.0		0.05310	−1.82									115.3	2.173
925B	26.78	35.93	8.166	286.6	19.59	0.07268	−1.64	20.36	0.10	20.30	0.10			20.33	0.25	113.8	1.567
664C	28.81	35.65	8.131	279.6	19.42	0.07139	−0.96	20.32	0.11	20.29	0.12	20.36	0.12	20.32	0.25	116.0	1.626
668B	29.54	35.51	8.154	292.7	19.81	0.07673	−1.70	20.78	0.11	20.69	0.11	20.75	0.10	20.74	0.25	112.4	1.466
999A	28.63	35.39	8.163	291.1	19.79	0.07564	−1.75	20.62	0.10	20.71	0.09			20.67	0.25	119.5	1.582
806B	30.36	34.75	8.129	279.7	19.55	0.07254	−2.04	20.13	0.22	20.20	0.17	20.62	0.19	20.31	0.31	111.0	1.532
GeoB4216-1	19.51	36.76	8.200	258.5		0.06434										121.6	1.891
GeoB1208-2	22.86	35.54	8.156	250.6		0.06272										112.0	1.787
G. sacculifer (with sac-like chamber, 500–600 μm)																	
851B[f]	23.78	34.81	8.017	196.6		0.04725	−1.49									73.1	1.549
925B	24.40	35.86	8.138	263.9	19.03	0.06596	−1.04	19.91	0.08	19.98	0.10			19.95	0.25	92.5	1.404
664C	26.81	35.84	8.130	268.8	19.15	0.06778	−0.62	19.81	0.11	19.83	0.11			19.82	0.25	90.0	1.262
668B	27.27	35.55	8.110	248.4	18.80	0.06359	−1.22	19.43	0.12					19.43	0.25	83.8	1.319
999A-1	27.31	35.79	8.158	284.7	19.57	0.07289	−1.08	20.17	0.14	20.40	0.14			20.28	0.25	97.5	1.339
999A-2					19.57			20.19	0.15	20.07	0.16			20.13	0.25		
999A-3					19.57			20.06	0.13	19.93	0.18	20.05	0.20	20.02	0.25		
806B	28.03	34.85	8.100	255.7	18.98	0.06516	−1.84	19.71	0.08	19.68	0.08	19.42	0.18	19.60	0.25	75.2	1.155
N. dutertrei (425–500 μm)																	
851B	18.73	34.84	7.950	147.4	16.28	0.0345	0.13	15.57	0.17	15.46	0.15			15.52	0.25	47.6	1.380
925B	18.85	35.72	8.073	210.8	17.83	0.0503	−0.86	16.93	0.13	17.01	0.12			16.97	0.25	61.7	1.229
999A	24.23	36.70	8.148	269.8	19.12	0.0665	−0.50	17.13	0.11	16.89	0.10			17.01	0.25	56.1	0.845
664C	22.16	36.27	8.128	243.6	18.57	0.0594	−0.58	17.03	0.11	16.71	0.12	16.95	0.12	16.90	0.25	59.7	1.006
C. wuellerstorfi (250–500 μm)																	
BOFS11K	3.73	34.92	8.049	119.3	16.24	0.03283		16.30	0.28	16.46	0.22	16.25	0.23	16.33	0.25	238.7	7.276
C. mundulus (250–500 μm)																	
BOFS17K	5.29	35.04	8.058	126.3	16.29	0.03338		16.41	0.16	16.50	0.16	16.25	0.14	16.39	0.25	171.5	5.144

[a] Location of sediment core. All environmental parameters taken from nearby GLODAP site (see Fig. 1 for location).
[b] Uncertainty in B/Ca ratio is 5% at 95% confidence.
[c] Oxygen isotope data were measured by M. Segl at the stable isotope Lab of the MARUM Center for Marine Environmental Sciences, Bremen on a Thermo Finnigan MAT252 coupled with a Thermo Finnigan Bremen-type carbonate device.
[d] Uncertainty in $\delta^{11}B$ measurement is either 2 s.e. (2 standard errors=2 standard deviations / square root of number of analyses) if >3 analyses and/or 0.25‰ if <2 analyses or if 0.25‰ is greater than the 2 s.e.
[e] $\delta^{18}O$ for *G. ruber* (white, 250–300 μm).
[f] $\delta^{18}O$ for *G. sacculifer* (with sac-like chamber, 300–355 μm).

parameters. To do this the effects of recent ocean acidification need to be removed (see Sabine et al., 2004). This can be readily achieved using the data set compiled by the Global Ocean Data Analysis Project (GLODAP; Key et al., 2004). The sites used for estimates of the Holocene carbonate system are shown in Fig. 1. All relevant equations are as listed in Zeebe and Wolf-Gladrow (2001) and in accordance with other studies of this kind the carbonic acid dissociation constants (K_1 and K_2) from Mehrbach et al. (1973) refitted by Dickson and Millero (1987) and the total pH scale are used throughout. Carbonate system calculations, including corrections relating to pressure, were performed using the CO_2sys.xls (version 12) program of Pelletier et al. (2005). Total boron concentrations in seawater were calculated from salinity using $[B]_{tot}$ (μmol/kg)=416×salinity (psu)/35 (Uppstrom, 1974).

In accordance with the oxygen isotope studies of Schmidt and Mulitza (2002) and Farmer et al. (2007) *G. ruber* (white) is assumed to inhabit the mixed layer throughout its life cycle and *G. sacculifer* (with sac-like chamber) is assumed to precipitate 70% of its calcite in the mixed layer and 30% (representing the calcite deposited during gametogenesis) at mid-thermocline depths. Compared to *G. ruber* and *G. sacculifer* the habitat depth for *N. dutertrei* is quite poorly constrained and here it is assumed to calcify at mid-thermocline depths (Farmer et al., 2007) Both *G. sacculifer* and *N. dutertrei* undergo depth migration during their life cycle, to reflect this an uncertainty of ±30 m is placed on the mid-thermocline habitat. Given these habitat depths a comparison is then possible between the documented ocean carbonate system relevant for each of these species and the measured $\delta^{11}B$ and B/Ca ratio. Fig. 2 shows a plot of depth vs. pH, the calculated $\delta^{11}B$ of $B(OH)_4^-$ and several other environmental parameters from the GLODAP and World Ocean Atlas (WOA05) databases for these sites where appropriate.

It should be noted that the WOA05 temperature and salinity data shown in Fig. 2 probably represent a good average of Late Holocene environmental parameters. Unfortunately measurements of temperature, salinity and the parameters required for a full characterisation of the carbonate system are much rarer than measurements of just temperature and salinity and consequently the carbonate system data from the GLODAP database represents a much shorter term snapshot of ocean conditions, for instance, in most cases the relevant data were collected during a single cruise. The GLODAP data set of Key et al. (2004) is however the best available compilation of concurrently measured T, S, DIC and TA and hence is used here. Regardless of these limitations, because the majority of the sites examined here are from tropical latitudes, seasonal variations are small and consequently the GLODAP data are likely to be representative of the average conditions. For most of the chosen GLODAP sites the temperature structure is similar to the long term mean and surface temperatures are generally within 1.5 °C of the WOA05 data providing confidence in this assertion (Fig. 2).

2.5. Caribbean oceanography and ODP Site 999A

There are two recognisable water masses that comprise the upper portions of the modern water column in the Caribbean Sea: the relatively fresh Caribbean Water (CW, 0–80 m) and the higher salinity Subtropical Under Water (SUW, 80–180 m). The latter forms the permanent thermocline and originates in the subtropical gyre of the

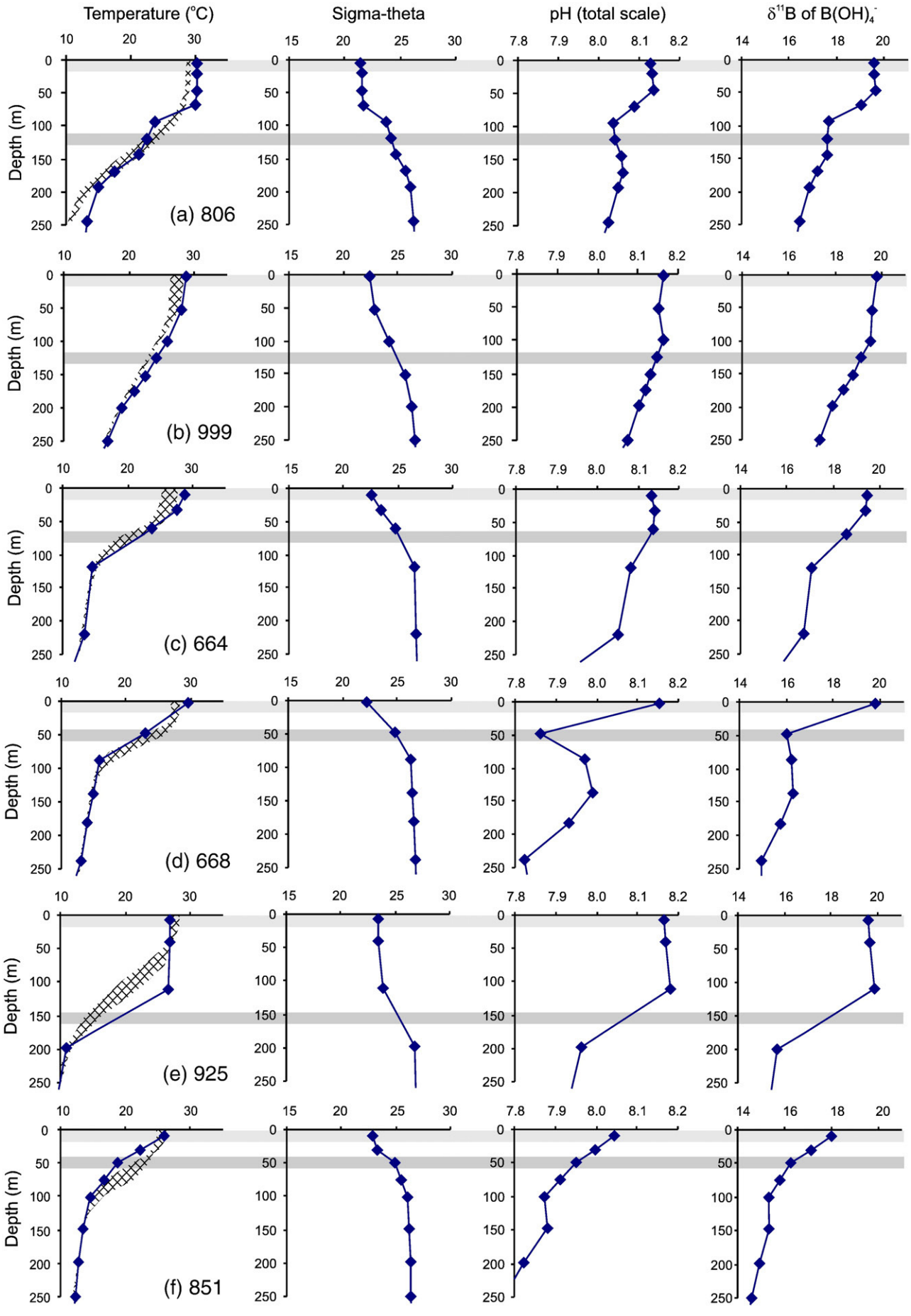
Temperature (°C)
Sigma-theta
pH (total scale)
δ11B of B(OH)4-
Depth (m)
(a) 806
(b) 999
(c) 664
(d) 668
(e) 925
(f) 851

North Atlantic (Wüst, 1964). Caribbean Water is a mixture of Amazon and Orinoco River river water with equatorial Atlantic surface water and is delivered to the Caribbean Sea by the Guyana Current (a mixture of the North Brazil Current and the North Equatorial Current) via passages between the Antilles Islands (Hellweger and Gordon, 2002). Surface water flow in the Caribbean Current is westward and water leaves the Caribbean Sea through the Yucatan Channel into the Gulf of Mexico. To the east of ~70 °W fresh water input from the Orinoco and Amazon has a significant influence on Sea Surface Salinity (SSS) variations (Hellweger and Gordon, 2002) and enhances biological productivity (Corredor and Morell, 2001). In the western Caribbean where Site 999A is located changes in the position of the Intertropical Convergence Zone (ITCZ) cause a distinct dry and wet season (Dessier and Donguy, 1994). In wet season (August–October) the ITCZ is at its most northerly position (6–10 °N) resulting in a relatively large freshwater input into the Caribbean via run off and direct precipitation. The amount of Atlantic water flowing into the Caribbean is reduced during this time due to the waning of the Guyana Current due to the development of a retroflection known as the North Equatorial Counter Current (Johns et al., 2002). During the dry season (February–May) the ITCZ reaches it's most southerly position centred over the Amazon River basin. Surface water flow through the Caribbean is enhanced at this time (Johns et al., 2002) by the development of strong easterly winds (Morrison and Smith, 1990) and coastal upwelling of relatively nutrient poor water (belonging to the SUW) is induced in the southern Caribbean Sea (Corredor, 1979).

The concentration of CO_2 in the modern surface water of the Caribbean is largely close to equilibrium with the atmosphere (Takahashi et al., 2002) but it does exhibit small seasonal variations (±10–20 ppm) in tandem with small variations in SST. Wanninkhof et al. (2007) calculate that the net annual flux of CO_2 is negative and the Caribbean Sea accounts for 0.04% to 1% of global oceanic CO_2 uptake. It is important to note that on a finer scale the southwestern part of the Caribbean, where ODP Site 999A is located, is a near year-round minor source of CO_2 to the atmosphere with air-sea differences in pCO_2 of around 0 ppm in the winter and spring and 10–20 ppm in the summer and autumn (Olsen et al., 2004).

3. Results and discussion

3.1. Core top calibration of $\delta^{11}B$ and the generation of pH estimates

Fig. 3 shows a comparison between the predicted $\delta^{11}B$ value of $B(OH)_4^-$ at the habitat depth of each foraminiferal sample and the measured $\delta^{11}B$. A full list of the $\delta^{11}B$ data can be found in Table 2. The isotopic composition of the foraminifera analysed here and the calculated isotopic composition of $B(OH)_4^-$ in seawater at their habitat depth are similar (Fig. 3). For the shallower dwelling species (*G. sacculifer* and *G. ruber*) there appears to be a near constant offset between the measured and predicted values of ~0.8‰. This offset to higher $\delta^{11}B$ probably relates to the effect of the photosynthetic activity of the symbionts these species harbour, which modify the micro-environment around the foraminifera (e.g. Wolf-Gladow et al., 1999; Zeebe et al., 2003). The measured isotopic offset equates to a micro-environment around *G. ruber* that is ~0.07 pH units more basic than seawater. This offset is not as extreme as predicted by Zeebe et al. (2003) but is in the correct direction. The two epifaunal benthic species do not harbour symbionts and consequently the measured $\delta^{11}B$ is identical to the predicted value. For *N. dutertrei* the relationship between the measured and predicted $\delta^{11}B$ is partly obscured by uncertainties relating to the habitat depth but on average the measured value is ~1.5‰ lighter than predicted. This offset toward lower pH is consistent with models for species lacking a high density of active symbionts where the micro-environment is more influenced by foraminiferal respiration and calcification which makes it more acidic than the surrounding seawater (Wolf-Gladow et al., 1999; Zeebe et al., 2003).

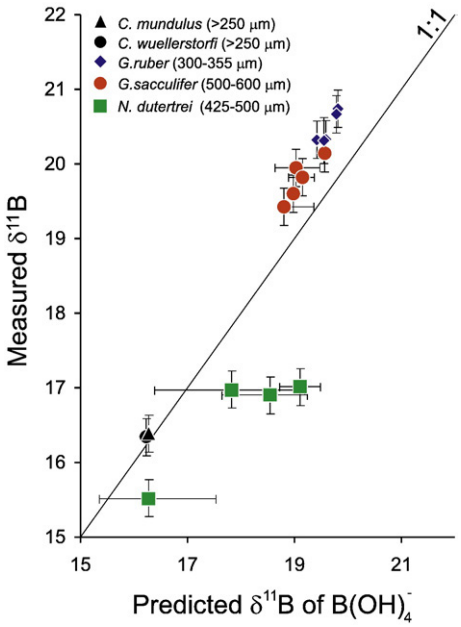

Fig. 3. Predicted $\delta^{11}B$ of $B(OH)_4^-$ vs. measured $\delta^{11}B$ for *G. sacculifer* (with sac, 500–600 μm), *G. ruber* (white, 300–355 μm), *N. dutertrei* (425–500 μm), *C. wuellerstorfi* (>250 μm) and *C. mundulus* (>250 μm) from a variety of locations. The predicted $\delta^{11}B$ were calculated using the pre-industrial carbonate system parameters at the depth at which the foraminifera calcify and a $^{11-10}K_B = 1.0272$ (Klochko et al., 2006). Error bars indicate the level of uncertainty in the $\delta^{11}B$ measurement (Table 2) and for *G. Sacculifer* and *N. dutertrei* error bars also reflect an uncertainty of ±30 m in the habitat depth for this species (see text). Note that the uneven shape of these depth related error bars is due to the shape of the $\delta^{11}B$ of $B(OH)_4^-$ profile and in some instances it is smaller than the symbol (see Fig. 2).

The general coherency of the data set, despite quite large variations in bottom water $CaCO_3$ saturation state (Table 1 and Fig. 4) also implies that secondary effects, such as preservation, are not as important in determining the boron isotopic composition of foraminifera as has previously been invoked (e.g. Wara et al., 2003; Hönisch and Hemming 2004; Ni et al., 2007).

The general disagreement between this data set and other published $\delta^{11}B$ values for foraminifera (e.g. Hönisch et al., 2007; Ni et al., 2007; Fig. 5) suggests that the accuracy of NTIMS approaches may be compromised. A detailed comparison of NTIMS and MC-ICPMS methods of foraminiferal analysis is beyond the scope of this manuscript but will be dealt with in a subsequent paper (Ni et al. in preparation). Nonetheless a brief discussion of analytical discrepancies is warranted here.

Empirical calibrations of cultured foraminifera, corals and inorganically precipitated calcites all measured in the same laboratory (Hönisch et al., 2007) have been used to argue that the most applicable isotopic equilibrium value for marine carbonates is that of Kakihana et al. (1977; 1.0194). However, as mentioned earlier, the recently determined value for seawater is 1.0272±0.0006 (Klochko et al., 2006), leading Klochko et al. (2006) to propose that species vital effects, and particularly the modification of micro-environments surrounding the organically precipitated

Fig. 2. Depth vs. temperature, density (sigma theta), pre-industrial pH from GLODAP stations near the cores studied here and the predicted $\delta^{11}B$ of $B(OH)_4^-$ using these parameters and a $^{11-10}K_B = 1.0272$ (Klochko et al., 2006; see Fig. 1 for locations). Grey horizontal bars indicate the assumed depth habitats for *G. ruber* (top), *G. sacculifer* (70% top, 30% bottom) and *N. dutertrei* (bottom). The cross hatched area on each temperature profile encompasses the seasonal mean (Jan–Mar, Apr–Jun, Jul–Sep, Oct–Dec) temperatures from the WOA05 dataset.

Table 3
Down core data for *G. ruber* (white, 300–355 μm) from ODP Site 999A

Depth	Age [a]	$\delta^{11}B$							B/Ca	pH	T[c]	S[d]	TA_{SAL}[e]	$[CO_3^{2-}]_{SAL}$[f]	CO_2sw_{SAL}	$[CO_3^{2-}]_{B/Ca}$[g]	$pCO_2sw_{B/Ca}$
(cmbs)	(kyr)	1	2 s.e.	2	2 s.e.	3	2 s.e.	Av[b]	(μmol/mol)		(°C)	psu	(μmol/kg)	(μmol/kg)	(ppm)	(μmol/kg)	(ppm)
4.5	3.9	20.62	0.10	20.71	0.09			20.67	119.5	8.172	28.3	35.5	2330	296	274	288	266
11	4.6	21.01	0.09	20.72	0.06	20.62	0.08	20.79		8.181	28.5	35.0	2301	296	264		
14.5	5.0	20.66	0.11	20.52	0.08			20.59	122.9	8.172	28.1	35.0	2301	289	272	280	264
31	7.8	20.85	0.09	20.79	0.09			20.82	128.0	8.185	28.3	35.6	2333	302	264	286	250
31	7.8	20.71	0.11	20.73	0.11			20.72	126.8	8.177	28.3	35.6	2333	299	270	284	257
39	9.5	20.62	0.09	20.73	0.09			20.68	118.1	8.179	27.5	36.1	2366	301	272	292	264
43	10.3	20.96	0.09	20.89	0.12			20.93	120.9	8.197	27.5	36.4	2384	313	259	299	248
48	11.7	20.76	0.10	20.68	0.10			20.72	111.7	8.187	26.9	36.5	2390	305	268	301	265
57	14.0	21.07	0.09	20.88	0.09			20.98	124.9	8.200	27.3	36.8	2408	319	258	299	242
61	15.1	20.95	0.10	21.08	0.09			21.02	116.5	8.201	27.4	37.1	2425	323	258	310	248
61	15.1	21.09	0.11	21.21	0.10			21.15	119.8	8.211	27.4	37.1	2425	328	251	311	238
71	17.3	21.00	0.08	21.09	0.08			21.04	112.6	8.213	26.5	37.1	2426	322	251	313	244
82	19.2	21.71	0.12	21.79	0.10			21.75	110.8	8.271	26.0	37.0	2419	346	210	336	204
93	21.1	21.31	0.07	21.13	0.07	21.24	0.08	21.23		8.235	25.7	37.0	2416	324	235		
102	22.5	21.15	0.07	21.37	0.08			21.26	111.1	8.230	26.4	37.2	2430	331	239	322	232
113	24.8	21.59	0.10	21.43	0.07			21.51	108.6	8.252	26.2	37.1	2422	338	223	331	218
120	26.3	21.55	0.11	21.70	0.12			21.62	104.7	8.262	26.1	36.8	2410	340	215	338	214
120	26.3	21.80	0.09	21.59	0.08			21.69	109.3	8.267	26.1	36.8	2410	343	212	335	207
172	36.9	21.00	0.10	21.24	0.09			21.12	116.1	8.225	26.3	36.5	2387	318	240	309	233
213	47.1	21.21	0.10	21.12	0.08			21.16	109.1	8.231	26.2	36.3	2378	318	235	317	235
234	52.3	21.42	0.12	21.17	0.10			21.29	112.3	8.239	26.3	36.2	2372	322	229	318	226
271	61.4	21.42	0.08	21.20	0.14			21.31	107.1	8.233	26.6	36.8	2407	329	234	326	232
331	76.3	20.92	0.08	20.85	0.10			20.89	112.7	8.209	26.6	35.5	2330	301	247	301	248
356	83.0	21.02	0.08	20.75	0.13			20.88	111.2	8.210	26.6	35.1	2308	297	245	301	248
373	88.1	20.60	0.10	20.76	0.10			20.68	107.1	8.183	27.2	36.1	2366	300	269	303	272
413	99.6	20.57	0.11	20.58	0.12			20.58	111.6	8.179	27.0	35.7	2342	292	271	300	278
433.5	104.5	20.67	0.10	20.85	0.11			20.76	125.6	8.200	26.7	35.2	2311	293	253	299	257
474	114.2	20.35	0.13	20.16	0.15			20.26	104.9	8.164	26.6	34.8	2289	272	279	286	294
482	116.1	20.13	0.14	20.23	0.15			20.18	109.6	8.152	27.1	34.7	2280	269	288	273	293
494	119.1	20.24	0.11	20.00	0.10			20.12	103.4	8.146	27.3	34.6	2277	266	293	264	290
504	122.3	20.81	0.11	20.70	0.10			20.75	118.7	8.176	28.5	35.7	2339	301	271	287	258
523	131.0	20.64	0.10	20.70	0.15			20.67	110.8	8.159	29.1	36.2	2372	305	286	302	283

[a] Age in thousands of years using the age model of Schmidt et al. (2004).
[b] Average $\delta^{11}B$. Uncertainty is +/− 0.25‰.
[c] Mg/Ca derived temperature from Schmidt et al. (2004).
[d] Salinity reconstructed as detailed in Schmidt et al. (2004).
[e] Total alkalinity determined from salinity and the modern salinity TA relationship in the surface Caribbean (TA=59.19*Salinity+229.08).
[f] $[CO_3^{2-}]$ determined from TA from salinity and pH.
[g] $[CO_3^{2-}]$ determined iteratively using pH and B/Ca (see text for details).

calcite, are responsible for the disagreement between the empirically derived value of Hönisch et al. (2007) and the experimentally determined value. One factor that is not considered by the critical review of boron isotopes by Pagani et al. (2005) nor addressed by Klochko et al. (2006), is the assumption that reported boron isotope values by NTIMS are accurate to within the quoted precision. As discussed by Foster et al. (2006), the ~4‰ range in $\delta^{11}B$ reported for similar core top foraminifera samples documents that for NTIMS measurements this is not the case. Notably, seawater $\delta^{11}B$ values reported by those laboratories commonly measuring marine carbonates by NTIMS are consistently in the range 39.5±0.6‰ (see Palmer et al., 1998; Hönisch et al., 2003; Gonfiantini et al., 2003; Aggarwal et al., 2004; Hönisch and Hemming 2004; Foster et al., 2006) which is in good agreement with what is reported here (39.50±0.19‰; 2 s.d.; n=7; Table A2) and by positive TIMS methodologies (as summarised in Aggarwal et al., 2004).

NTIMS approaches require an ionisation enhancing matrix to be added to the normalising NIST SRM 951 boric acid standard, and because boron-free seawater (prepared using column chemistry) is commonly used for this, the agreement of all laboratories for seawater is perhaps not surprising. Thus the contrast between the standard matrix and the foraminiferal carbonate sample matrix may play a role in generating inter-laboratory biases in foraminiferal $\delta^{11}B$ by NTIMS. As is discussed in detail in the Online supplementary material, the sample matrix has no influence on the $\delta^{11}B$ generated by MC-ICPMS since it is removed prior to analysis. Work at Bristol has noted that a key factor in causing inaccurate $\delta^{11}B$ by TE-NTIMS (Total evaporation NTIMS) is the inferred presence of organic material. Such organics are inadequately oxidised during standard cleaning protocols, presumably as they are released from the interior of the test by dissolution. Over the course of several months, TE-NTIMS $\delta^{11}B$ analyses of the same solutions of dissolved foraminifera become lighter by up to

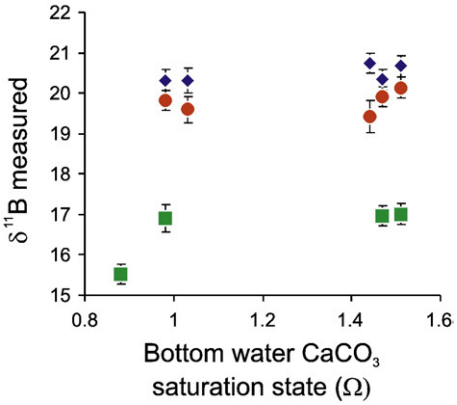

Fig. 4. Measured $\delta^{11}B$ for *G. ruber*, *G. sacculifer*, and *N. dutertrei* for the sites examined here plotted against bottom water $CaCO_3$ saturation state (Ω) from a nearby GLODAP site.

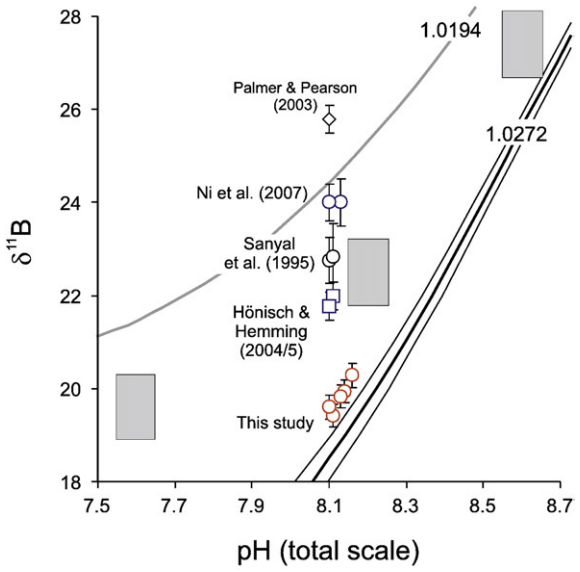

Fig. 5. pH dependence of the boron isotopic composition of $B(OH)_4^-$ for $^{11-10}K_B = 1.0272 \pm 0.0006$ (Klochko et al., 2006) and 1.0194 (Kakihana et al., 1977) at 25 °C and 35 psu. Also shown here are Holocene *G. sacculifer* from the Atlantic and Pacific oceans from several sources determined using NTIMS (Sanyal et al., 1995; Palmer and Pearson, 2003; Hönisch and Hemming, 2004, 2005; Ni et al., 2007) along with cultured *G. sacculifer* data of Sanyal et al. (2001; grey boxes). The *G. sacculifer* data that are part of the core top calibration (Fig. 3) are also shown (red circles) and clearly follow the $^{11-10}K_B = 1.0272$ curve with a slight offset to higher pH (see text). Due to the constraint that this figure can only be plotted at a single temperature and salinity other data from the core top calibration have not been plotted. For the examples from the literature the pH has been recalculated as outlined in the text using nearby GLODAP data sites. (For interpretation of the references to colour in this figure legend, the reader is referred to the web version of this article.)

6‰. This change is attributed to the result of acid hydrolysis of the organics by the solutions in which they are stored. Protocols specifically aimed at breaking down this organic material prior to measurement bring the $\delta^{11}B$ by TE-NTIMS to within 1 ± 1‰ of the MC-ICPMS values for the same samples.

In contrast to the existing NTIMS data (e.g. Hönisch et al., 2007), Fig. 3 suggests that boron isotopes in marine carbonates such as foraminifera, when measured by MC-ICPMS, adhere well with our understanding of the boron isotope system. For instance, after the minor 0.8‰ correction due to symbiont activity, it is relatively straight forward to convert a $\delta^{11}B$ measurement of *G. ruber* to a pH, provided temperature and salinity are known. The following equation (modified from Zeebe and Wolf-Gladow, 2001) will be used throughout the rest of this contribution:

$$pH = pK_b^* - \log\left[-\frac{\delta^{11}B_{sw} - (\delta^{11}B_{ruber} - 0.8)}{\delta^{11}B_{sw} - \left(1.0272 \times \left(\delta^{11}B_{ruber} - 0.8\right)\right) - 27.2}\right] \quad (6)$$

where pK_b^* is the pK^* value for boric acid at the in situ temperature and salinity, $\delta^{11}B_{sw}$ is the isotopic composition of seawater ($\delta^{11}B = 39.5$‰) and $\delta^{11}B_{ruber}$ is the measured isotopic composition of *G. ruber*.

3.2. B/Ca calibration and empirical relationships

As discussed previously the B/Ca ratio of foraminifera should be dependent on the partition coefficient of boron between seawater and calcite and proportional to the $[B(OH)_4^-/HCO_3^-]$ ratio of the seawater from which they precipitated. Fig. 6 shows the measured B/Ca ratio of the three species investigated here plotted against the calculated pre-industrial $[B(OH)_4^-/HCO_3^-]$ ratio at the relevant habitat depths (all B/Ca data can be found in Table 2). Clearly there is a first order relationship between the species but within an individual species a range of K_D's are required to account for the observed spread in B/Ca. Yu et al. (2007a) demonstrated, in a core top calibration of *G. bulloides* and *G. inflata* collected on a latitudinal transect of the North Atlantic from 60–30 °N, that there was a significant temperature and/or carbonate ion control on the incorporation of boron into foraminiferal carbonate. Fig. 7 shows the variation of the K_D with temperature and $[CO_3^{2-}]$ for the species examined here. The trends shown in Fig. 7 are in an opposite sense to those shown by Yu et al. (2007a) for *G. inflata* and *G. bulloides* but similar, for $[CO_3^{2-}]$, to their down core study of *G. ruber*. This contrasting behaviour perhaps indicates that the secondary controls on boron incorporation are species specific. One factor that requires further study is the role played by growth rate variations, which Ni et al. (2007) suggest influences the B/Ca ratio in *G. ruber* and *G. sacculifer*. Additional work is clearly needed to understand the causes of this behaviour but this is unfortunately beyond the scope of this contribution, nonetheless, these observations complicate the application of B/Ca in planktic foraminifera to trace changes in the carbonate system and serve to highlight the difficulties of calibrating a proxy using core top data alone.

One way in which the influence of environmental factors can be deconvolved is to examine the down core data at Site 999A and the published data for *G. ruber* from Site 668B (Yu et al., 2007a). Yu et al. (2007a) and Wara et al. (2003) showed a positive correlation between down core Mg/Ca derived SST and B/Ca ratio for *G. ruber* and *G. sacculifer*, respectively (Fig. 7c). Both sets of authors used these correlations to imply that there is a temperature control on the incorporation of boron into these species. As evident in Fig. 7a, there is a good correlation between the K_D of B/Ca and temperature for core top *G. ruber*. Yet, the B/Ca data for this species from the last 130 kyr at Site 999A (Table 3 and Fig. 8) and the last 440 kyr at Site 668B (from Yu et al., 2007a), although well correlated, clearly define a different slope to the core top data (Fig. 7c). This implies that temperature itself is not the most important influence on the boron incorporation into *G. ruber* and instead, based on the core top calibration, it seems most likely that $[CO_3^{2-}]$ is the dominant secondary environmental control on B/Ca. As will be discussed in more detail below, the colder glacial climate is

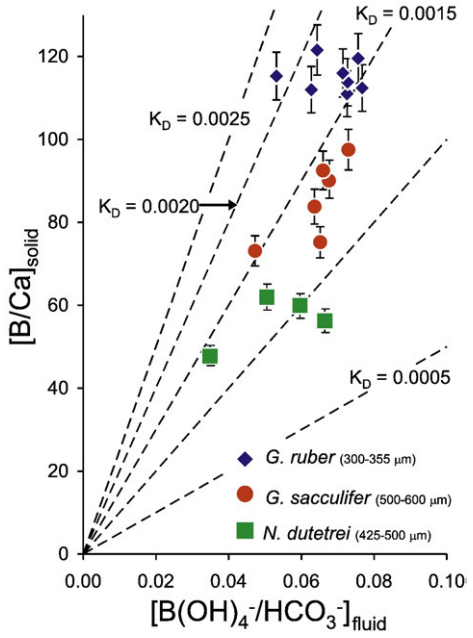

Fig. 6. B/Ca vs. seawater $[B(OH)_4^-/HCO_3^-]$ at habitat depth for *G. sacculifer* (with sac, 500–600 μm), *G. ruber* (white, 300–355 μm), *N. dutertrei* (425–500 μm). Error bars indicate the level of uncertainty associated with the B/Ca measurement (5%; 95% confidence).

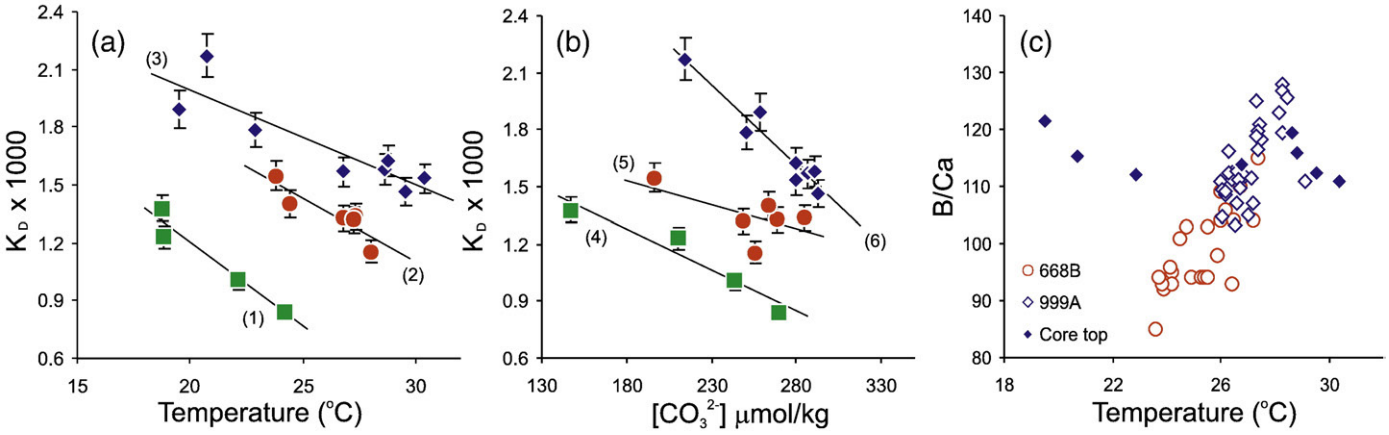

Fig. 7. Variations of B/Ca K_D with seawater (a) temperature (b) $[CO_3^{2-}]$ at the depth of habitat. Also shown are linear regressions through the data as follows: (1) $y=-0.0856x+2.912$, $R^2=0.94$, $n=4$; (2) $y=-0.0654x+3.0661$, $R^2=0.79$, $n=6$; (3) $y=-0.0488x+2.9677$, $R^2=0.78$, $n=8$; (4) $y=-0.00433x+2.0592$, $R^2=0.94$, $n=4$; (5) $y=-0.00255x+1.9937$, $R^2=0.36$, $n=6$; (6) $y=-0.00842x+3.9708$, $R^2=0.93$, $n=8$. (c) Measured B/Ca in *G. ruber* for down core 999A (Table 3) ODP Site 668B (Yu et al., 2007a) and the various core tops investigated here against sea surface temperature.

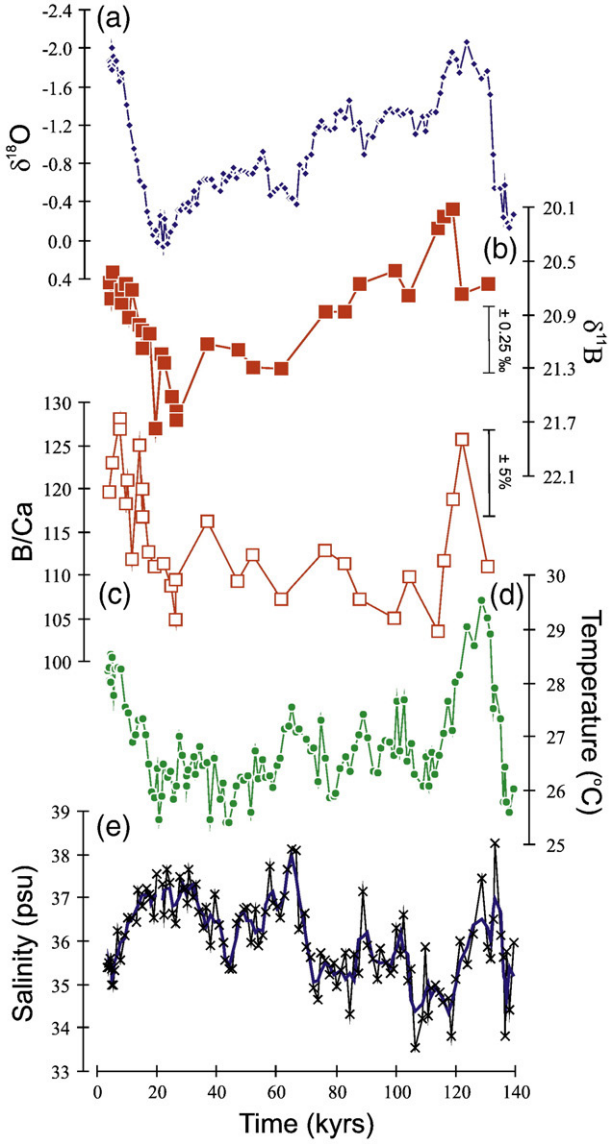

Fig. 8. (a) $\delta^{18}O$ (Schmidt et al., 2004), (b) $\delta^{11}B$ and (c) B/Ca for *G. ruber* (white, 300–355 µm) from ODP Site 999A, (d) Mg/Ca derived temperature for the same site and using the same species from Schmidt et al. (2004). (e) Salinity (psu) from Schimdt et al. (2004a) reconstructed using the data in (a) and (d).

characterised by higher $[CO_3^{2-}]$ in surface water than the Holocene, consequently the lower B/Ca during cold intervals is not temperature controlled but instead is a result of higher $[CO_3^{2-}]$ leading to a lower K_D (see Fig. 7b).

3.3. Variations in the carbonate system in Caribbean Sea over the last 130 kyrs

3.3.1. Down core $\delta^{11}B$ and pH variations at Site 999A

The $\delta^{11}B$ of *G. ruber* (white; 300–355 µm) from ODP Site 999A are shown in Fig. 8 and listed in Table 3. Note that several samples are full procedural duplicates and, in all cases, the $\delta^{11}B$ of the duplicates agree to within 0.15‰ (Fig. 8). Using Eq. (6), and the Mg/Ca and $\delta^{18}O$ derived temperature and salinity reconstructions of Schmidt et al. (2004), this $\delta^{11}B$ record can be converted to pH (Fig. 9) with an uncertainty that is dominated by the uncertainty in the boron isotope measurement, which roughly equates to ±0.02 pH units. The samples in the time series that are complete procedural duplicates agree within 0.015 pH units (see Table 3 and Fig. 9). These data indicate that pH changes in the Caribbean are largely synchronous with changes in ice volume as recorded by $\delta^{18}O$ over the last 130 kyr. Similar pH values to today are found through the Holocene and the early parts of marine isotope stage (MIS) 5 with progressively more basic values from MIS 5 to MIS 3, reaching a maximum value of 8.27 during MIS 2 before rapidly returning to Holocene values (8.17) during the deglaciation (Fig. 9).

Fig. 9 also shows a plot of Caribbean surface water pH along with the partial pressure of CO_2 in the atmospheric (pCO_2atm) from the Vostok ice core over the same period. Clearly there is a relationship between the two records suggesting that the carbonate system at Site 999A is changing in sympathy with pCO_2atm. In order to examine this situation further it is necessary to estimate the pCO_2 of the seawater and to do this an additional parameter form the carbonate system is needed.

3.3.2. Estimates of the second parameter of the carbonate system—constraints on $[CO_3^{2-}]$ from B/Ca ratio

In the modern ocean total alkalinity (TA) is linearly correlated with salinity (Fig. 10 for surface water in the Caribbean). This relationship arises because TA is the charge balance between the major conservative cations and anions in seawater, and this charge balance varies with salinity. Consequently, it is common for studies of this kind to make the assumption that the modern salinity–alkalinity relationship holds for the past ocean so that TA can be estimated from reconstructions of salinity (e.g. Palmer and Pearson, 2003; Hönisch and Hemming, 2005). Following these studies, a first order estimate of

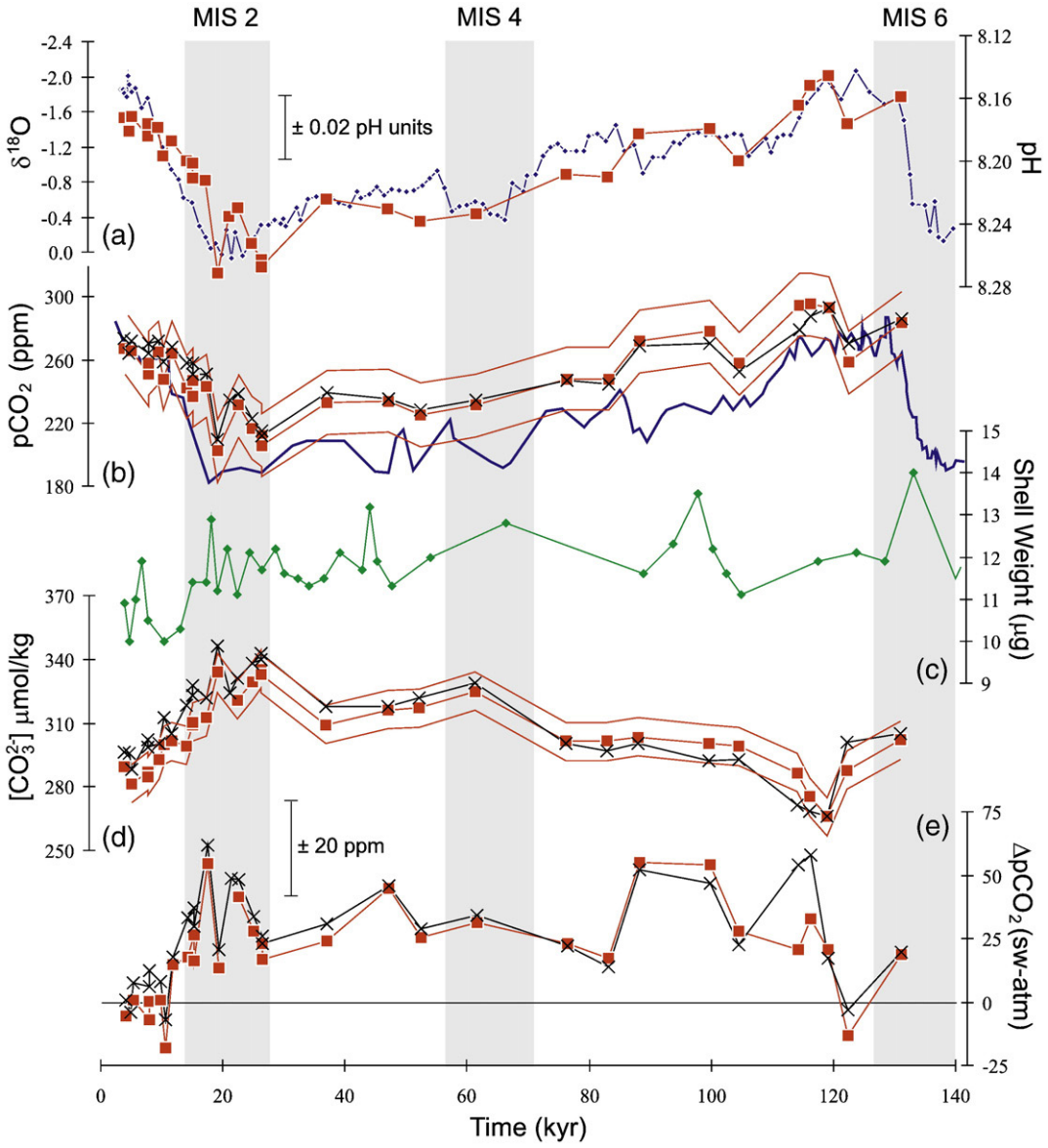

Fig. 9. (a) $\delta^{18}O$ (Schmidt et al., 2004; blue) and pH (red) derived from the $\delta^{11}B$, temperature and salinity record shown in Fig. 8. (b) pCO_2 for the atmosphere over the last 130 kyr from the Vostok ice core (blue line; Petit et al., 1999) and the calculated pCO_2sw at Site 999A (red). Red boxes are pCO_2sw reconstructed using $[CO_3^{2-}]$ from B/Ca, black crosses are pCO_2sw reconstructed by scaling TA with salinity reconstructed at this site by Schmidt et al. (2004). Uncertainty in pCO_2sw is ±20 ppm and is represented by the thin red lines. (c) Average test weight of *G. ruber* (white, 250–350 µm) from Schmidt et al. (2006). (d) $[CO_3^{2-}]$ µmol/kg reconstructed using measured B/Ca ratio in *G. ruber* in addition to the pH reconstruction based on $\delta^{11}B$. Uncertainty in this reconstruction is shown by the thin red lines and is ±9 µmol/kg. Black crosses are the $[CO_3^{2-}]$ reconstructed from scaling TA with salinity. (e) ΔpCO_2 (seawater–atmosphere) at Site 999A for the last 130 kyr. Symbols are the same as for (d). The grey vertical bars indicate glacial periods and are labelled with the appropriate marine isotope stage (MIS). Isotope stage boundaries are from Bassinot et al. (1994).

$[CO_3^{2-}]$ can be made by using the relationship shown in Fig. 10, the salinity reconstruction for Site 999A from Schmidt et al. (2004; Fig. 8), and the $\delta^{11}B$ derived pH record shown in Fig. 9. The uncertainty in this reconstruction, based on the uncertainty in the pH reconstruction, is ±10 µmol/kg (Fig. 9).

Given the understanding of the controls on the B/Ca ratio in core top *G. ruber* outlined above, coupled with the pH reconstruction from boron isotopes and temperature and salinity for Site 999A, it is possible, for the first time, to examine the accuracy of this salinity based $[CO_3^{2-}]$ reconstruction in detail. Fig. 7 shows that the K_D of B/Ca is dependent on $[CO_3^{2-}]$ therefore for a given pH (derived from $\delta^{11}B$) the $[CO_3^{2-}]$ necessary to generate the observed B/Ca ratio can be determined iteratively (see Fig. 9). An uncertainty of ±5% in the measured B/Ca results in an average uncertainty in $[CO_3^{2-}]$ of approximately ±5 µmol/kg. Uncertainty in the pH reconstruction of ±0.015 pH units equates to an uncertainty in $[CO_3^{2-}]$ of approximately ±7 µmol/kg. A quadratic addition of these gives an approximate total uncertainty in the $[CO_3^{2-}]$ reconstruction of ±9 µmol/kg. Fig. 9 shows that the $[CO_3^{2-}]$ calculated from B/Ca varies in a similar fashion to pH and agrees well with the $[CO_3^{2-}]$ calculated from pH and scaling TA with local salinity (Schmidt et al., 2004), varying from as low as 280 µmol/kg during the Holocene and MIS 5 to around 335 µmol/kg during the last glacial maximum (LGM). The influence of foraminiferal growth rate variations on this reconstruction are potentially problematic, since $[CO_3^{2-}]$ is thought to effect foraminiferal growth rate (as expressed as final shell weight; Barker and Elderfield, 2002; Bijma et al., 2002) and, as outlined above growth rate influences B/Ca ratio (see Ni et al., 2007). However, any influence of growth rate is incorporated in the core top calibration (Fig. 7) and is likely to be small — e.g. Bijma et al. (2002) demonstrate that shell weight of *G. sacculifer* grown in culture increases 3 µg for every 100 µmol/kg increase of $[CO_3^{2-}]$. If a similar

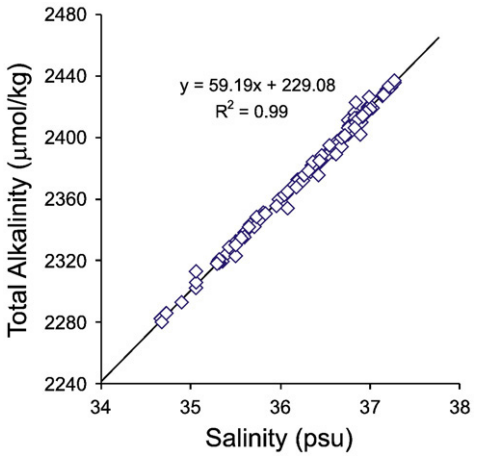

Fig. 10. A cross plot of surface water (0–200 m) total alkalinity (TA; µmol/kg) against salinity (psu) for the Caribbean Sea (11–20 °N and 68–62 °W). The data are from the data set complied by the GLODAP project (Key et al., 2004).

dependency is applied to *G. ruber* then the ~55 µmol/kg increase in $[CO_3^{2-}]$ for Site 999A during the LGM relates to a 1.65 µg increase in shell weight (~10% change in mass). Although actual measurements of shell weight are complicated by the effects of differential dissolution, the shell weight record for *G. ruber* (250–350 µm) from Site 999A shows a similarly small variation around the average weight (11.7 µg±1.6; 2 s.d; Schmidt et al., 2006) over the period investigated here, suggesting changes in growth rate of the order necessary to influence B/Ca did not occur and hence the B/Ca derived $[CO_3^{2-}]$ record is accurate within the quoted uncertainties.

3.3.3. pCO_2sw at Site 999A

Given these reconstructions it is possible to determine directly the pCO_2sw of the surface water using the equations listed in Zeebe and Wolf-Gladow (2001). Uncertainties in pCO_2sw are dominated by uncertainties in the pH and $[CO_3^{2-}]$ reconstructions, which combine to give an overall uncertainty of approximately ±20 ppm (Fig. 9). Within this level of uncertainty it is not important which $[CO_3^{2-}]$ reconstruction is used as both yield similar results (Fig. 9). A comparison between pCO_2sw and pCO_2atm from the Vostok ice core shows a good first order agreement (Fig. 9). However in detail there are several periods, most notably during the LGM and deglaciation and at around 90 kyr, where pCO_2sw values are significantly higher than the atmosphere. To examine this feature in more detail Fig. 9 shows the difference between pCO_2sw and pCO_2atm (ΔpCO_2; roughly equal to the magnitude of sea to air flux of CO_2). During the warm periods with high pCO_2atm (MIS 1 and 5e) the Caribbean Sea at Site 999A was close to equilibrium with the atmosphere with respect to CO_2 (Fig. 9). However, during the colder periods with lower SSTs Site 999A was a source of CO_2 to the atmosphere with $\Delta pCO_2 > 20$ ppm, with several periods where the seawater had a partial pressure of CO_2 in excess of the atmosphere by 50–70 ppm (Fig. 9).

The modern surface ocean consists of regions where the concentration of CO_2 in the surface water is close to equilibrium with the atmosphere and parts where the concentration is higher (a source to the atmosphere) and lower (a sink) compared to the atmosphere. Those parts of the modern surface ocean that are sources of CO_2 to the atmosphere are areas where deep waters, rich in respired nutrients, upwell (Takahashi et al., 2002). This suggests that at those times where ΔpCO_2 is positive at Site 999A the nutrient and DIC concentration of the surface waters at Site 999A were increased.

Modelling studies (e.g. Schiller et al., 1997) and several paleorecords (e.g. Peterson and Haug, 2006) suggest that the mean position of the Atlantic ITCZ migrated southwards during cold periods such as the last glacial maximum. This would have had the effect of shifting the mean climate state of the region toward the climate currently seen during the modern dry season (February–May) where inflow into the Caribbean is highest and upwelling occurs along the southern coast (Corredor, 1979). It is possible therefore that an expansion of this coastal upwelling, induced by the southward shift in the ITCZ, generally stronger glacial winds and a shallower glacial thermocline in the Western Atlantic (Slowey and Curry, 1995; Mulitza et al., 1997), could encompass Site 999A causing the elevated ΔpCO_2 observed. Support for this hypothesis comes from nanofossil analysis, which suggests that surface water at Site 999A did become enriched in nutrients (+DIC) during several periods over the last 130 kyr which coincide with maxima in ΔpCO_2 (Kameo et al., 2004). Kameo et al. (2004) also argued that increased nutrient delivery from the Amazon and Orinoco river systems may be responsible for enhancing the nutrient concentration of the surface waters in the Caribbean. However, in the modern Caribbean, although the Amazon/Orinoco freshwater plume does cause enhanced productivity (Corredor and Morell, 2001) it is associated with a pCO_2sw drawdown rather than an increase (Wanninkhof et al., 2007).

In a regional study of the $[CO_2]_{aq}$ of surface water in the southern Equatorial Atlantic using compound specific $\delta^{13}C$ measurements, Benthien et al. (2005) noted that during the LGM the Brazil current, which forms part of the western boundary current that flows into the Caribbean via the Guyana current, had a ΔpCO_2 of ~80 ppm—much higher than the Holocene situation where this area is in near equilibrium with the atmosphere (Takahashi et al., 2002). Similarly high ΔpCO_2 was also found in the western Equatorial Atlantic (Benthien et al., 2005) which may have been a consequence of increased upwelling in the Eastern Equatorial Atlantic (e.g. Wefer et al., 1996) and an advection of this signal westwards. Therefore the elevated ΔpCO_2 at Site 999A during the LGM and other cold periods may reflect the changing ΔpCO_2 of the subtropical gyre water that flows into the Caribbean rather than simply changes in upwelling local to the Caribbean.

Similar changes in ΔpCO_2, as described here for the Caribbean and the southern Equatorial Atlantic, have also been recorded at the LGM for the Central Equatorial Pacific (Jasper et al., 1994) and again, whilst pCO_2sw is generally lower than the Holocene, ΔpCO_2 is higher than its present value. The modern equatorial ocean is a significant source of CO_2 to the atmosphere (Millero, 2006). If the size of this source was enhanced during MIS 2–5 then mechanisms previously proposed for lowering pCO_2atm, such as Fe fertilisation of the Southern Ocean (Martin, 1990) or carbon sequestration to deep ocean reservoirs (e.g. Sigman and Boyle, 2000), must be even more efficient than most models suppose. This is a particularly salient point because even the most complex of models fails to reconstruct a low enough glacial pCO_2 through simulating those mechanisms thought to be most important (e.g. dust fertilisation of the Southern Ocean and circulation changes; Brovkin et al., 2007). Clearly, further studies of this kind are required to examine whether the phenomena described here for the Caribbean occur in other parts of the oceans, but if such reorganisation of the carbonate system did occur globally then the difficulty of reconstructing glacial pCO_2 may be further compounded.

4. Conclusions

In this contribution it has been demonstrated that the MC-ICPMS analysis of the boron isotopic composition of marine carbonates represents a major step forward in the application of the boron isotope-pH proxy. The good agreement between the isotopic composition of $B(OH)_4^-$ in seawater and the measured isotopic composition of a variety of foraminiferal species suggests that the model for boron incorporation into marine carbonates proposed by Hemming and Hanson (1992) is sound and, following the recent

experimental determination of $^{11-10}K_B$, the boron isotope pH proxy now has a firm grounding. In combination with the calibrated B/Ca proxy, it has also been shown that the $\delta^{11}B$ in *G. ruber* provides constraints on the reorganisations of the ocean carbonate system that occurred in the Caribbean Sea over the last 130 kyrs. By applying these proxies to other areas and by extending them to planktic species living at high latitudes (such as *Neogloboquadrina pachyderma*) and to benthic species (such as *C. wuellerstofi*) it will be possible to determine the ocean carbonate system response to the waxing and waning of the Quaternary ice sheets and ultimately gain insights into the mechanisms responsible.

Acknowledgements

The Natural Environment Research Council is thanked for providing funding for this contribution in the form of a NERC fellowship to GLF. Chris Coath is acknowledged for his vital assistance in the laboratory and Tim Elliott, Daniela Schmidt, Andy Ridgwell, Derek Vance, James Rae, and Erica Hendy are thanked for comments on an earlier draft of this manuscript. The IODP, Barbara Donner (RCOM), Jimin Yu and Harry Elderfield (Cambridge University) are also gratefully acknowledged for supplying the samples used in this study. Mathew Schmidt is thanked for supplying an electronic copy of his 999A salinity and foram weight data. This manuscript was significantly improved by the comments of two anonymous reviewers and by the efficient editorial handling of Harry Elderfield.

Appendix A. Supplementary data

Supplementary data associated with this article can be found, in the online version, at doi:10.1016/j.epsl.2008.04.015.

References

Aggarwal, J.K., Mezger, K., Pernicka, E., Meixner, A., 2004. The effect of instrumental mass bias on $\delta^{11}B$ measurements: a comparison between thermal ionisation mass spectrometry and multiple-collector ICP-MS. Int. J. Mass Spectrom. 232, 259–263.
Archer, D., Winguth, A., Lea, D.W., Mahowald, N., 2000. What caused the glacial/interglacial atmospheric pCO_2 cycles. Rev. Geophys. 38, 159–189.
Barker, S., Elderfield, H., 2002. Foraminiferal calcification response to glacial–interglacial changes in atmospheric CO_2. Science 297, 833–836.
Barker, S., Greaves, M., Elderfield, H., 2003. A study of cleaning procedures used for foraminiferal Mg/Ca paleothermometry. Geochem. Geophys. Geosys. 4, 8407. doi:10.1029/2003GC000559.
Barker, S.A., Kiefer, T., Elderfield, H., 2004. Temporal changes in North Atlantic circulation constrained by planktonic foraminiferal shell weights. Paleoceanography 19, PA3008. doi:10.1029/2004PA001004.
Bassinot, F.C., et al., 1994. The astronomical theory of climate and the age of the Brunhes–Matuyama magnetic reversal. Earth Planet. Sci. Lett. 126, 91–108.
Benthien, A., et al., 2005. The carbon isotopic record of the $C_{37:2}$ alkenone in the South Atlantic: Last Glacial Maximum (LGM) vs. Holocene. Palaeogeogr. Palaeoclimatol. Palaeoecol. 221, 123–140.
Bickert, T., Curry, W.B., Wefer, G., 1997. Late Pliocene to Holocene (2.6–0) western Equatorial Atlantic deep-water circulation: inferences from benthic stable isotopes. In: Shackleton, N.J., Curry, W.B., Richter, C., Bralower, T.J. (Eds.), Proceedings of the Ocean Drilling Program, Scientific Results, 154. Ocean Drilling Program, College Station, TX, pp. 239–254.
Bijma, J., Hönisch, B., Zeebe, R.E., 2002. Impact of the ocean carbonate chemistry on living foraminiferal shell weight: comment on "Carbonate ion concentration in glacial-age deep waters of the Caribbean Sea" by W. S. Broecker and E. Clark. Geochem. Geophys. Geosyst. 3, 1064. doi:10.1029/2002GC000388.
Bird, M.I., Cali, J., 2002. A revised high-resolution oxygen-isotope chronology for ODP-668B: implications for Quaternary biomass burning in Africa. Glob. Planet. Change 33, 73–76.
Boyle, E.A., Keigwin, L.D., 1985/86. Comparison of Atlantic and Pacific paleochemical records for the last 215,000 years: changes in deep ocean circulation and chemical inventories. Earth Planet. Sci. Lett. 76, 135–150.
Brovkin, V., Ganopolski, A., Archer, D., Rahmstorf, S., 2007. Lowering of glacial atmospheric CO_2 in response to changes in oceanic circulation and marine biogeochemistry. Paleoceanography 22, PA4202. doi:10.1029/2006PA001380.
Catanzaro, E.J., et al., 1970. Boric Assay; Isotopic, and Assay Standard Reference Materials, vol. 260-17. US National Bureau of Standards. Special Publication.
Corredor, J.E., 1979. Phytoplankton response to low level nutrient enrichment through upwelling in the Columbian Caribbean Basin. Deep-Sea Res. 26A, 731–741.
Corredor, J.E., Morell, J.M., 2001. Seasonal variation of physical and biogeochemical features in eastern Caribbean Surface Water. J. Geophy. Res. 106 (C3), 4517–4525.
Dessier, A., Donguy, J.R., 1994. The sea surface salinity in the tropical Atlantic between 10°S and 30°N—seasonal and interannual variations (1977–1989). Deep-Sea Res. 41 (1), 81–100.
Dickson, A.G., Millero, F.J., 1987. A comparison of the equilibrium constants for the dissociation of carbonic acid in seawater media. Deep-Sea Res. 34, 1733–1743.
DOE, 1994. Handbook of Methods for The Analysis of The Various Parameters of the Carbon Dioxide System in Sea Water; Version 2. ORNL/CDIAC-74.
Farmer, E.C., Kaplan, A., de Menocal, P.B., Lynch-Stieglitz, J., 2007. Corroborating ecological depth preferences of planktonic foraminifera in the tropical Atlantic with the stable oxygen isotope ratios of core top species. Paleoceanography 22, PA3205. doi:10.1029/2006PA001361.
Foster, G.L., Ni, Y., Haley, B., Elliott, T., 2006. Accurate and precise isotopic measurement of sub-nanogram sized samples of foraminiferal hosted boron by total evaporation NTIMS. Chem. Geol. 230, 161–174.
Freudenthal, T., Meggers, H., Henderiks, J., Kuhlmann, H., 2002. Upwelling intensity and filament activity off Morocco during the last 250,000 years. Deep-Sea Res., Part 2 49, 3655–3674.
Gonfiantini, R., et al., 2003. Intercomparison of boron isotope and concentration measurements. Part 2: evaluation of results. Geostand. Newsl. 27, 41–57.
Hellweger, F.L., Gordon, A.L., 2002. Tracing Amazon River water into the Caribbean Sea. J. Mar. Res. 60, 537–549.
Hemming, N.G., Hanson, G.N., 1992. Boron isotopic composition and concentration in modern marine carbonates. Geochim. Cosmochim. Acta 56, 537–543.
Hönisch, B., et al., 2003. The influence of symbiont photosynthesis on the boron isotopic composition of foraminifera shells. Mar. Micropalentol. 928, 1–10.
Hönisch, B., Hemming, N.G., 2004. Ground-truthing the boron isotope—paleo *p*H proxy in planktonic foraminifera shells: partial dissolution and shell size effects. Paleoceanography 19, PA4010. doi:10.1029/2004PA001026.
Hönisch, B., Hemming, N.G., 2005. Surface ocean pH response to variations in pCO_2 through two full glacial cycles. Earth Planet. Sci. Lett. 236, 305–314.
Hönisch, B., Hemming, N.G., Loose, B., 2007. Comment on "A critical evaluation of the boron isotope-pH proxy: the accuracy of ancient ocean pH estimates" by M. Pagani, D. Lemarchand, A. Spivak, J. Gaillardet. Geochim. Cosmochim. Acta 71, 1636–1641.
Jasper, J.P., Hayes, J.M., Mix, A.C., Prahl, F.G., 1994. Photosynthetic fractionation of ^{13}C and concentrations of dissolved CO_2 in the central equatorial Pacific during the last 255,000 years. Paleoceanography 9, 781–798.
Johns, W.E., T.L., T., Fratantoni, D.M., Wilson, W.D., 2002. On the Atlantic inflow to the Caribbean Sea. Deep-Sea Res. 49, 211–243.
Kakihana, H., Kotaka, M., Satoh, S., Nomura, M., Okamoto, M., 1977. Fundamental studies on the ion-exchange separation of boron isotopes. Chem. Soc. Jpn., B 50, 158–163.
Kameo, K., et al., 2004. Glacial–interglacial surface water variations in the Caribbean Sea during the last 300 ky based on calcareous nannofossil analysis. Palaeogeogr. Palaeoclimatol. Palaeoecol. 212, 65–76.
Key, R.M., et al., 2004. A global ocean carbon climatology: results from Global Data Analysis Project (GLODAP). Glob. Biogeochem. Cycles 18, GB4031. doi:10.1029/2004GB002247.
Klochko, K., Kaufman, A.J., Yoa, W., Byrne, R.H., Tossell, J.A., 2006. Experimental measurement of boron isotope fractionation in seawater. Earth Planet. Sci. Lett. 248, 261–270.
Lea, D.W., Pak, D.K., Spero, H.J., 2000. Climate impact of Late Quaternary Equatorial Pacific sea surface temperature variations. Science 289, 1719–1724.
Manighetti, B., McCave, I.N., 1995. Late glacial and Holocene palaeocurrents around Rockall Bank, NE Atlantic Ocean. Paleoceanography 10, 611–626.
Martin, J., 1990. Glacial–interglacial CO_2 change: the iron hypothesis. Paleoceanography 5, 1–13.
Mehrbach, C.C., Culberson, H., Hawley, J.E., Pytkowicz, R.M., 1973. Measurement of the apparent dissociation constant of carbonic acid in seawater at atmospheric pressure. Limno. Oceanogr. 18, 897–907.
Millero, F.J., 2006. Chemical Oceanography, Marine Science Series. CRC Press, Boca Raton.
Morrison, J.M., Smith, O.P., 1990. Geostrophic transport variability along the Aves Ridge in the eastern Caribbean Sea during 1985 and 1986. J. Geophys. Res. 95, 699–710.
Mulitza, S., Dürkoop, A., Hale, W., Wefer, G., Niebler, H.S., 1997. Planktonic foraminifera as recorders of past surface-water stratification. Geology, 25 (4), 335–338.
Ni, Y., et al., 2007. A core top assessment of proxies for the ocean carbonate system in surface-dwelling foraminifers. Paleoceanography 22, PA3212. doi:10.1029/2006PA001337.
Olsen, A., Trinanes, J.A., Wanninkhof, R., 2004. Sea-air flux of CO_2 in the Caribbean Sea estimated using in situ and remote sensing data. Remote Sens. Environ. 89, 309–325.
Pagani, M., Lemarchand, D., Spivack, A., Gaillardet, J., 2005. A critical evaluation of the boron isotope-*p*H proxy: the accuracy of ancient *p*H estimates. Geochim. Cosmochim. Acta 69, 953–961.
Palmer, M.R., Pearson, P.N., 2003. A 23,000-year record of surface water pH and PCO_2 in the Western Equatorial Pacific Ocean. Science 300, 480–482.
Palmer, M.R., Pearson, P.N., Cobb, S.J., 1998. Reconstructing past ocean pH-depth profiles. Science 282, 1468–1471.
Pearson, P.N., Palmer, M.R., 2000. Atmospheric carbon dioxide concentrations over the past 60 million years. Nature 406, 695–699.
Pelletier, G., Lewis, E. and Wallace, D., 2005. A calculator for the CO_2 system in seawater for Microsoft Excel/VBA. Washington State Department of Ecology, Olympia, WA, Brookhaven National Laboratory Upton, NY.
Peterson, L.C., Haug, G.H., 2006. Variability in the mean latitude of the Atlantic Intertropical Convergence Zone as recorded by rivering input of sediments to the Cariaco Basin (Venezuela). Paleogeog. Paleoclim. Palaeoecol. 234, 97–113.
Petit, J.R., et al., 1999. Climate and atmospheric history of the past 420,000 years from the Vostok ice core, Antarctica. Nature 399, 429–436.

Raymo, M.E., Oppo, D.W., Curry, W., 1997. The mid-Pleistocene climate transition: a deep sea carbon isotopic perspective. Paleoceanography 12, 546–559.
Sabine, C.L., et al., 2004. The oceanic sink for anthropogenic CO_2. Science 305, 367–371.
Sanchez-Valle, C., et al., 2005. Boron isotopic fractionation between minerals and fluids: new insights from *in situ* high pressure-high temperature vibrational spectroscopic data. Geochim. Cosmochim. Acta 69, 4301–4313.
Sanyal, A., Hemming, N.G., Hanson, G.N., Broecker, W.S., 1995. Evidence for a higher pH in the glacial ocean from boron isotopes in foraminifera. Nature 373, 234–236.
Sanyal, A., Nugent, M., Reeder, R.J., Bijma, J., 2000. Seawater pH control on the boron isotopic composition of calcite: evidence from inorganic calcite precipitation experiments. Geochim. Cosmochim. Acta 64, 1551–1555.
Sanyal, A., Bijman, J., Spero, H., Lea, D.W., 2001. Empirical relationship between pH and the boron isotopic composition of *Globigerinoides sacculifer*: implications for the boron isotope paleo-pH proxy. Paleoceanography 16, 515–519.
Schiller, A., Mikolajewicz, U., Voss, R., 1997. The stability of the North Atlantic thermohaline circulation in a couple ocean–atmosphere general circulation model. Clim. Dyn. 13, 325–347.
Schmidt, G.A., Mulitza, S., 2002. Global calibration of ecological models for planktic foraminifera from coretop carbonate oxygen-18. Mar. Micropaleontol. 44, 125–140.
Schmidt, M.W., Spero, H.J., Lea, D.W., 2004. Links between salinity variation in the Caribbean and North Atlantic thermohaline circulation. Nature 428, 160–163.
Schmidt, M.W., Vautravers, M.J., Spero, H.J., 2006. Western Caribbean sea surface temperatures during the late Quaternary. Geochem. Geophys. Geosys. 7, Q02P10. doi:10.1029/2005GC000957.
Shackleton, N.J., Crowhurst, S.J., Hagelberg, T., Pisias, N.G., Schneider, D.A., 1995. A new Late Neogene time scale: application to Leg 138 sites. In: Pisias, N.G., Mayer, L.A., Palmer-Julson, A., van Andel, T.H. (Eds.), Proceedings of the Ocean Drilling Program, Scientific Results, 138. Ocean Drilling Program, College Station, TX, pp. 73–101.
Siegenthaler, U., et al., 2005. Stable carbon cycle–climate relationship during the Late Pleistocene. Science 310, 1313–1317.
Sigman, D.M., Boyle, E.A., 2000. Glacial/interglacial variations in atmospheric carbon dioxide. Nature 407, 859–869.
Slowey, N.C., Curry, W.B., 1995. Glacial–interglacial differences in circulation and carbon cycling within the upper western North Atlantic. Paleoceanography 10, 715–732.
Takahashi, T., et al., 2002. Global sea–air CO_2 flux based on climatological surface ocean pCO_2, and seasonal biological and temperature effects. Deep-Sea Res., Part 2 49, 1601–1622.
Thiessen, W., Bleil, U., 2002. Age model of sediment core GeoB1208-2. Pangaea. doi:10.1594/Pangaea.66375.
Toggweiler, J.R., Russell, J.L., Carson, S.R., 2006. Midlatitude westerlies, atmospheric CO_2, and climate change during the ice ages. Paleoceanography 21, PA2005. doi:10.1029/2005PA001154.
Uppstrom, L.R., 1974. Boron/chlorinity ratio of deep-sea water from pacific ocean. Deep-Sea Res. Oceanogr. Abstr. 21, 161–162.
Wara, M.W., Delaney, M.L., Bullen, T.D., Ravelo, A.C., 2003. Possible roles pH, temperature, and partial dissolution in determining boron concentration and isotopic composition in planktonic foraminifera. Paleoceanography 18, PA1100. doi:10.1029/2002PA000797.
Wanninkhof, R., Olsen, A., Trinanes, J.A., 2007. Air–sea CO_2 fluxes in the Caribbean Sea from 2002–2004. J. Mar. Sys. 66, 272–284.
Wefer, G., et al., 1996. Late Quaternary surface circulation of the South Atlantic: the stable isotope record and implications for heat transport and productivity. In: Wefer, G., Berger, W.H., Siedler, G., Webb, D.J. (Eds.), The South Atlantic: Present and Past Circulation. Springer-Verlag, Berlin, pp. 461–502. Heidelberg.
Wolf-Gladow, D.A., Bijma, J., Zeebe, R.E., 1999. Model simulation of the carbonate chemistry in the microenvironment of symbiont bearing foraminifera. Mar. Chem. 64, 181–198.
Wüst, G., 1964. Stratification and Circulation in the Antilean–Caribbean Basins, Part 1: Spreading and Mixing of the Water Types With an Oceanographic Atlas. Columbia University Press, New York.
Yu, J., Elderfield, H., 2007. Benthic foraminiferal B/Ca ratios reflect deep water carbonate saturation state. Earth Planet. Sci. Lett. 258, 73–86.
Yu, J., Elderfield, H., Hoenisch, B., 2007a. B/Ca in planktonic foraminifera as a proxy for surface seawater pH. Paleoceanography 22, PA2202. doi:10.1029/2006PA001347.
Yu, J., Elderfield, H., Greaves, M., Day, J., 2007b. Preferential dissolution of benthic foraminiferal calcite during laboratory reductive cleaning. Geochem. Geophys. Geosys. Q06016. doi:10.1029/2006GC001571.
Zeebe, R., 2005. Stable boron isotope fractionation between dissolved $B(OH)_3$ and $B(OH)_4^-$. Geochim. Cosmochim. Acta 69, 2753–2766.
Zeebe, R., Wolf-Gladow, D.A., 2001. CO_2 in Seawater: Equilibrium, Kinetics, Isotopes. . Elsevier Oceanography Series, vol. 65. Elsevier, Amsterdam.
Zeebe, R.E., Wolf-Gladrow, D.A., Bijma, J., Hönisch, B., 2003. Vital effects in foraminifera do not compromise the use of $\delta^{11}B$ as a paleo-*p*H indicator: evidence from modeling. Paleoceanography 18, PA1043. doi:10.1029/2003PA000881.